



ARF6 and r17-non-ARF6). To test the requirement of myristoylation for ARF binding and effective interactions with lipid bilayers, both myr-ARF6 and non-ARF6 were prepared in the presence of GDP. Interactions between ARF and PIP<sub>2</sub> have been reported, yet controversies have persisted (Antonny et al., 1997; Terui et al., 1994), so investigations were performed on myr-ARF6 binding to the membrane containing PIP<sub>2</sub> and to membranes in which PIP<sub>2</sub> was replaced by other negatively charged lipids, such as PI, PG, and PS. It is shown by spectral subtractions and NLLS fits that the main change in ESR spectra from the model membrane containing PIP<sub>2</sub> upon myr-ARF6 binding is the emergence or enhancement of sharp spectral components, which are superimposed on the main components.

The aim of this study is to correlate the sharp components in ESR spectra from spin-labeled membrane systems with defects in lipid bilayers. We provide evidence for defects in DPPC bilayers, associate them with sharp components in ESR spectra from DPPC membranes and then show that these sharp components can be significantly enhanced or reduced through lipid/lipid or lipid/protein interactions. By simple analogy, we suggest that the sharp components in the ESR spectra from the model membrane containing PIP<sub>2</sub> upon myr-ARF6 binding arise from defects in the bilayers induced or enhanced by specific interactions between myr-ARF6 and PIP<sub>2</sub>. The significance of defects induced by lipid-lipid and lipid-protein interactions in membrane vesiculation and membrane fusion processes, as well as the ability of ARF to modulate availability of substrate to PLD, are discussed.

## MATERIALS AND METHODS

### Expression and purification of recombinant ARF6 proteins

We expressed human ARF6 based on procedures developed by Hong et al. (1994) and Lodge et al. (1997). Cultures (4 ml) of transformed *Escherichia coli* were started directly from 15% glycerol stocks and grown for 13 h at 37°C in an air shaker at 200 RPM. For preparation of myr-ARF6, maintenance of both the ARF6 and *N*-myristoyl transferase plasmids was accomplished through dual antibiotic selection using 300 µg/ml carbenicillin and 112 µg/ml kanamycin. Preparation of non-ARF6 was conducted under carbenicillin selection at 300 µg/ml to maintain the ARF6 plasmid. These plasmids were generous gifts of Dr. Joel Moss at the National Institutes of Health. Cultures were spun to pellet bacteria, and pellets were washed twice in LB media. Pellets were resuspended in 4 ml of minimal medium (17 mM NaCl, 37 mM NH<sub>4</sub>Cl, 95 mM Na<sub>2</sub>HPO<sub>4</sub>, 17 mM K<sub>2</sub>HPO<sub>4</sub>, 2 mM MgSO<sub>4</sub>, 0.1 mM CaCl<sub>2</sub>, 0.4% glucose), and 1 ml was inoculated into 200 ml of minimal medium at identical antibiotic conditions. Cultures were grown at 37°C until OD<sub>600</sub> was between 0.6 and 0.9. The cultures (200 ml) were added directly to 4 L of minimal medium in a fermenter flask and grown at 37°C at 200 RPM and 20 L/min air flow. Myristic acid (200 mg dissolved in 100% ethanol and diluted to 3.3% ethanol in sterile water) was added 1:133 to the fermenter at an OD<sub>600</sub> of 0.6. At OD<sub>600</sub> 1.0, cells were induced at 0.3 mM isopropyl β-D-thiogalactopyranoside. Cultures were supplemented with 40 ml of 20% glucose and 930 mg of carbenicillin and 225 mg of kanamycin. Three hours after incubation, 400 ml of 1 M sterile sodium phosphate was added to cultures

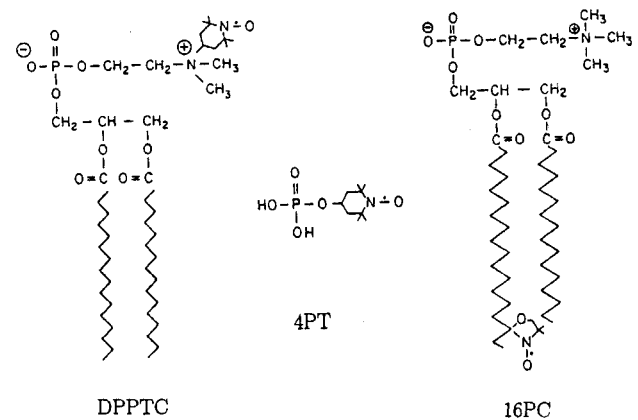


FIGURE 1 The chemical structures of spin label DPPTC, 4PT, and 16PC.

to maintain a neutral pH. Total induction time was 9 h. After induction, cells were pelleted by centrifugation, washed, and frozen at  $-80^{\circ}\text{C}$ .

The purification of ARF6 was accomplished using an adaptation of previous chromatographic methods (Randazzo et al., 1995; Brown and Sternweis, 1995). Cells were resuspended in lysis buffer (20 mM Tris, pH 8.0, 1 mM MgCl<sub>2</sub>, 1 mM dithiothreitol, 100 mM NaCl, 100 µM GDP), plus protease inhibitors (130 µM phenylmethylsulfonyl fluoride, 1 µg/ml pepstatin A, 1 µg/ml leupeptin, 1 µg/ml aprotinin, 10 µg/ml trypsin inhibitor, 20 µg/ml Na-P-tosyl-L-lysine chloromethyl ketone, 20 µg/ml *N*-tosyl-L-phenylalanine chloromethyl ketone). Lysozyme (4 mg) was added, and the cell suspension was frozen for 30 min at  $-80^{\circ}\text{C}$ . The cell suspension was thawed, 1 mg/ml of DNase was added, and samples were sonicated using a Sonic Dismembrator 550 (Fisher Scientific, Springfield NJ) probe sonicator (eight cycles alternating between on and off in 1-s intervals). Lysed cells were spun at  $100,000 \times g$  for 1 h. Supernatant was removed and diluted 1:4 in buffer (without NaCl) to reduce the NaCl concentration to a final concentration of 25 mM. The pellet was resuspended in lysis buffer (with 25 mM NaCl and 0.1% β-octyl-glucoside). The resuspended pellet was spun at  $100,000 \times g$  for 1 h. Supernatant was removed and combined with the first supernatant. ARF6 mixture was added to a 90-ml diethylaminoethyl-Sephacel column equilibrated with lysis buffer containing 25 mM NaCl. The flow-through and two column washes were collected (containing the ARF6). The flow-through and washes were concentrated to 1.5 ml using an Amicon concentrator with PM10 membrane. Concentrated ARF6 was applied to a 160-ml bed volume AcA44 gel filtration column, and proteins were chromatographically resolved in lysis buffer containing 25 mM NaCl. Fractions 72–84 containing the ARF6 were pooled and concentrated, typically to 2–5 mg/ml. The modified and unmodified proteins were compared by sodium dodecyl sulfate polyacrylamide gel electrophoresis using a gel shift assay (Franco et al., 1995). The ARF6 proteins were concentrated and stored at  $-80^{\circ}\text{C}$ . The purification of the recombinant CDC42 protein expressed in *E. coli* was accomplished essentially as described in Walker et al. (2000). The initial 17 amino acids corresponding to human ARF6 (r17-ARF6) were custom synthesized either with or without a myristic acid modification (Sigma Genosys).

### Preparation of ESR samples

#### Materials

Lipids POPE, DPPC, liver PI (sodium salt), DOPG (sodium salt), DOPS (sodium salt), and spin labels DPPTC, 5PC, 10PC, and 16PC (the chemical structure of 16PC is shown in Fig. 1) were purchased from Avanti (Alabaster, AL). Gm1 was purchased from Matreya (Pleasant Gap, PA). They

were used without further purification. PIP<sub>2</sub> (sodium salt) is a product of Roche Diagnostics Co. (Indianapolis, IN). Spin label 4PT (chemical structure shown in Fig. 1) was purchased from Aldrich (Milwaukee, WI) (at pH 7, 4PT is a water-soluble spin label but insoluble in the hydrophobic interior of bilayers). CHOL, CTB, and cytochrome C are products of Sigma Chemical Co. (St. Louis, MO).

### Preparation of dispersions and binding of proteins

The dispersion used in this study is composed of POPE, DPPC, CHOL, and PIP<sub>2</sub> at molar ratios of 114:11:1.6:6. Because this dispersion has been used for measuring PLD activity in an exogenous assay (detailed in Brown and Sternweis, 1995), in which the amount of PC hydrolyzed by PLD can be quantitatively controlled and measured, it was chosen as a model membrane for this study. In the following, unless otherwise specified, the dispersion refers to the model membrane with the above composition. Its preparation procedure is described as follows. Measured stock solutions of lipid (in chloroform, except for PIP<sub>2</sub> in chloroform:methanol 2:1 (v/v)) and of spin label were mixed thoroughly in a glass tube. The weight of dry lipids was 0.25 mg, and the concentration of spin label was 0.5 mol % of the total lipids. As the solvent was evaporated by N<sub>2</sub> flow, the dried lipids formed a thin film on the wall of the tube, and then the sample was evacuated with a mechanical pump overnight to remove trace amounts of solvent. After addition of 50  $\mu$ l of pH 7.0 Tris buffer (50 mM Tris, 160 mM NaCl, and 0.1 mM EDTA), the lipids were scraped off the wall and kept in the dark at room temperature for 2 h. The vesicle solution was vortexed for 1 min, and 10  $\mu$ l of the solution was then transferred into a capillary (ID 0.8–1.1 mm) for ESR measurement. For protein binding, after the dispersion was hydrated for 2 h, a calculated amount of protein solution was added, and the dispersion was vortexed for 1 min and applied for ESR measurements.

### Binding of CTB to a model membrane

The procedure to prepare the model membrane for CTB binding is similar to that described above. The composition of the membrane is DPPC (DSPC):Gm1:CHOL = 9(9):1:10. The concentration of the spin label 10PC is 0.5 mol % of total lipids (0.5 mg in weight). The dried lipid mixture was hydrated with 0.5 ml of pH 7.0 Tris buffer (50 mM Tris, 10 mM NaCl, and 0.1 mM EDTA) for 2 h. Meanwhile, CTB powder (2 g) was dissolved in 1 ml of deionized water, the resulting solution contains 1 mg of CTB, 50 mM Tris, 200 mM NaCl, 3 mM NaN<sub>3</sub>, and 1 mM EDTA. Then 10  $\mu$ l of the vesicle solution and 10  $\mu$ l of the CTB solution were mixed and transferred into a capillary (ID 0.8–1.1 mm) for ESR measurement.

### Preparation of LUVs of pure DOPC and of DOPC/PIP<sub>2</sub> at molar ratio of 95:5

The procedure for mixing DOPC, PIP<sub>2</sub> and the spin label DPPTC (0.5 mol % of total lipids) is the same as that for preparing the dispersions described above. The weight of total lipids is 2 mg, and 200  $\mu$ l of pH 7.0 Tris buffer (50 mM Tris, 160 mM NaCl, and 0.1 mM EDTA) was added to the dried lipid mixture. The lipids were scraped off the wall, and the vesicle solution was extruded through a stack of membrane filters with pore sizes of 0.4, 0.2, and 0.1  $\mu$ m (Millipore, Bedford, MA) in an extruder (Lipex Biomembranes, Vancouver, British Columbia, Canada) five times.

### ESR spectroscopy and NLLS analysis of ESR spectra

ESR spectra were obtained on a Bruker Instruments (Billerica, MA) EMX ESR spectrometer at a frequency of 9.34 GHz. All spectra were digitized

to 1024 points and had  $\sim$ 120 Gauss sweep widths. All spectra were taken at 23°C.

NLLS analyses of the spectra based on the stochastic Liouville equation (Meirovitch et al., 1982; Schneider and Freed, 1989) were performed using the latest version of the fitting program (Budil et al., 1996). They yield the following parameters: rotational diffusion rate  $R_{\perp}$  and order parameter  $S$ .  $R_{\perp}$  is the rotational diffusion rate of the nitroxide radical around an axis perpendicular to the mean symmetry axis for the rotation. This symmetry axis is also the direction of preferential orientation of the spin-labeled molecule (Schneider and Freed, 1989). For 5PC, 10PC, and 16PC,  $R_{\perp}$  represents the rotational wagging motion of the long axis of the acyl chains (Ge et al., 1994). For the headgroup label DPPTC, it represents the wagging motion of the ammonium group. For the simulation of ESR spectra of spin labels incorporated into MLVs, a MOMD model (Meirovitch et al., 1984; Budil et al., 1996) was used. This model is based on the characteristics of the dynamic structure of lipid dispersions; i.e., locally in a lipid bilayer fragment, lipid molecules are preferentially oriented by the structure of the bilayer, but globally, the lipid bilayer fragments are distributed randomly (Meirovitch et al., 1984). The order parameter  $S$  is a measure of the angular extent of the rotational diffusion of the nitroxide moiety. The larger the  $S$ , the more restricted is the motion, which means that laterally the lipid molecules are packed more tightly. Therefore,  $S$  reflects the local ordering of lipid molecules in the macroscopically disordered membrane dispersions. The magnetic  $A$ -tensor and  $g$ -tensor components needed for the simulations were obtained from fits to rigid limit spectra of the samples, which were taken at liquid nitrogen temperature.

### 4PT/VC assay

This assay is for measurement of permeability of lipid bilayers. A lipid dispersion (dry weight 2 mg) is prepared with 0.5 mol % 4PT and hydrated with 200  $\mu$ l of pH 7 Tris buffer (50 mM Tris, 10 mM NaCl, 0.1 mM EDTA), as described above, and 4  $\mu$ l of 200 mM VC aqueous solution is added to the dispersion. Because the amount of VC added is large enough to kill all the spin label in the dispersion, the supernatant will give no ESR signal. Whether an ESR signal can be detected from the pellet is determined by the permeability of the bilayers to VC molecules.

## RESULTS

### A preliminary ESR experiment

ESR spin labeling has proved to be a powerful technique for studying lipid-lipid (Ge et al., 1994; Shin and Freed, 1989) and lipid-protein (Ge and Freed, 1999; Patyal et al., 1997; Freed, 2000) interactions. To test to what extent the dynamic structure of the membrane could be perturbed by PLD activity, and in particular to test whether the ESR method is sensitive enough to detect these perturbations, a preliminary experiment on a model membrane (a dispersion) was performed. The dispersion,  $\sim$ 0.1 mg in weight, is composed of PE from liver, DPPC, a headgroup spin label DPPTC (its chemical structure is shown in Fig. 1), CHOL, and PIP<sub>2</sub> at a molar ratio of 114:5.5:5.5:1.6:6 (86%:8%:1%:5%). (The dispersion was buffered with 50 mM Na-HEPES (pH 7.5), 1 mM dithiothreitol, 80 mM KCl, 3 mM EGTA, 3 mM MgCl<sub>2</sub>, and 2 mM CaCl<sub>2</sub> in the presence of GTP $\gamma$ s, a partially purified preparation of ARF from brain, and protein kinase C of  $\alpha$ -isoform. The volume of the dispersion is 1 ml.) Plotted in Fig. 2 are ESR spectra of DPPTC from two test samples. The upper spectrum was taken from the

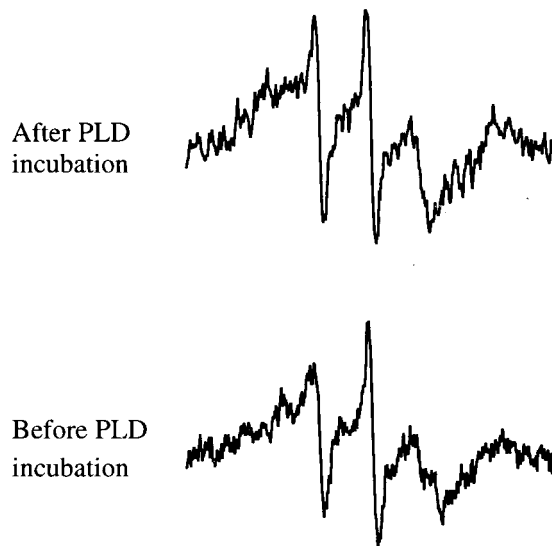


FIGURE 2 Results from a preliminary experiment. ESR spectra at 20°C of spin label DPPTC from two dispersion samples with the same composition: liver PE, DPPC, DPPTC, CHOL, PIP<sub>2</sub> of molar ratio 114:5.5:5.5:1.6:6 (0.86:0.04:0.04:0.01:0.05). The upper spectrum was taken from one sample that had been incubated in the presence of recombinant PLD1 (Sf21 expressed in cells) with 27% of DPPC being hydrolyzed, whereas the lower one is from another sample without any incubation with PLD1.

sample that had been incubated in the presence of PLD1 (expressed in Sf21 insect cell cytosol) causing 27% of the DPPC to be hydrolyzed, whereas the lower one was from another sample without incubation with PLD1. Both spectra are composed of two components, a narrower three-line spectrum superimposed on a very broad spectrum.

Because the sharper component is very similar to those that will be extensively involved in the ESR spectra we will present in this paper, we would like to distinguish between two different sources from which sharp components could be generated. 1) For spin labels dissolved in the bulk aqueous phase (source A), ESR spectra consist of three narrow hyperfine lines of nearly equal intensity, which result from fast tumbling motions of these spin labels (Carrington and McLachlan, 1967). 2) For spin labels dispersed in the bilayers (source B), ESR spectra appear narrower, hence sharper, relative to the main very broad component. This is because the local ordering is smaller and/or the motion is faster for the former than for the latter. At physiological temperatures, these relatively sharper components are nevertheless in the slow motional regime. In fact, our simulations show that the rotational diffusion rate and the order parameter for the sharper components of Fig. 2 are  $3.4 \times 10^8 \text{ s}^{-1}$  to  $5.2 \times 10^8 \text{ s}^{-1}$  and 0.11–0.18, respectively, which yield slow motional ESR spectra, (Schneider and Freed, 1989). The line shapes from source B can thus be easily distinguished from those of the fast motional spectra from source A, because they are broader and they show a significant

variation of widths and amplitudes for the three different hyperfine lines (cf. Fig. 2). In this study we are primarily interested in the sharper components from the membrane-bound spin labels (i.e., case 2), because they might be related to defect formation in the membranes.

A source for A spin labels could be water-soluble nitroxide radicals, such as those that could result from breakdown of spin-labeled lipids, or they could be spin labels that are separated out from the bilayers. However, in the latter case, the critical micelle concentration of DPPC is  $5 \times 10^{-10} \text{ M}$  (Israelachvili, 1991), which is very low. Introducing a nitroxide radical into DPPC, either attached to the acyl chain (e.g., 5PC, 10PC, or 16PC) or attached to the headgroup (e.g., DPPTC), might increase the CMC slightly. But even a factor of 10 increase to  $5 \times 10^{-9} \text{ M}$  in the aqueous phase is still well below the concentration of spin label, which can be detected by ESR spectroscopy,  $\sim 1 \times 10^{-7} \text{ M}$ . (The limit of the number of spins detectable by ESR spectroscopy as measured in our laboratory is 1 pmol ( $1 \times 10^{-12} \text{ mol}$ ). The typical volume of aqueous solution in an ESR lipid dispersion sample is 10  $\mu\text{l}$ , so the limit of concentration of spin label detected by ESR is  $1 \times 10^{-7} \text{ M}$ . This limit corresponds to an extremely weak, barely detectable signal, whereas we see substantial signals from the sharp components.) So it is impossible to observe any ESR signal from the PC-type spin labels in the aqueous phase simply because of their low CMC values.

The absence of any ESR spectra from A spin labels does not rule out the possibility that PLD cleaves not only DPPC molecules, generating choline, but also DPPTC spin labels, generating TEMPO-choline, which is an A spin label. Because TEMPO-choline is water soluble (it is known that both choline and TEMPO are water soluble; therefore, TEMPO-choline must be also water soluble), once produced it will be quickly reduced by the reducing agent,  $\text{NaN}_3$ , in the buffer. (The same is, of course, also true for any DPPTC in the buffered aqueous phase.) It is, however, difficult for the reducing agent to access the nitroxide moieties in the DPPTC in the membrane, which is why they can survive substantial periods.

It is seen from Fig. 2 that the relative intensity of the narrower component is slightly greater in the spectrum from the sample incubated with PLD1 than that without incubation with PLD1. This is a small but significant change, which demonstrates that ESR is sensitive to perturbations in membrane dynamic structure induced by PLD catalytic activity.

### General features of ESR spectra before and after myr-ARF6 and non-ARF6 bindings

A headgroup spin label, DPPTC, and three chain spin labels, 5PC, 10PC, and 16PC, were used to investigate

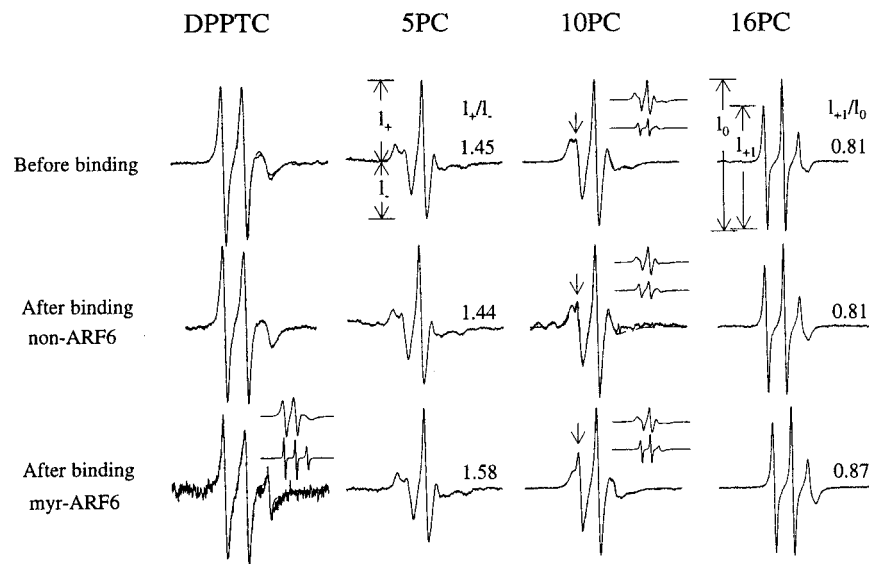


FIGURE 3 ESR spectra at 20°C from spin labels DPPTC, 5PC, 10PC, and 16PC in a dispersion composed of POPE:DPPTC:CHOL:PIP<sub>2</sub> of molar ratio 114:11:1.6:6 (0.86:0.08:0.01:0.05) before and after addition of myr-ARF6 and non-ARF6. The molar ratios of myr-ARF6/lipids and non-ARF6/lipids are 1700 and 1000, respectively. The experimental spectra are plotted in solid lines, whereas the simulations are in dashed lines. For each simulated spectrum, two components obtained from NLLS fitting are plotted at the upper right corner except the one from DPPTC before ARF6 binding, which was fit with only one component. The ratio of positive peak intensity  $I_+$  to negative peak intensity  $I_-$  of the central peak,  $I_+/I_-$ , measured for the spectra from 5PC, and the ratio of low-field line peak-peak intensity to central field line peak-peak intensity,  $I_{+1}/I_0$ , measured for the spectra from 10PC are indicated at each spectrum. The arrows indicate the sharp peaks in the spectra from 10PC.

effects of myr-ARF6 and non-ARF6 on the membrane dynamic structure when they bind to the membrane surface. The molar ratios of total lipids in the dispersion to proteins added are 1700 for myr-ARF6 binding and 1000 for non-ARF6 binding. ESR spectra from the four spin labels in the dispersion before and after myr- and non-ARF6 binding are shown in Fig. 3. The most notable changes in ESR spectra are the emergence of a sharper component in the spectrum from DPPTC and a significant increase in intensity of the sharper component in the spectrum from 10PC upon myr-ARF6 binding. In contrast, upon non-ARF6 binding there is only a slight change in intensity of the low-field peak relative to the central peak in the spectrum from DPPTC and a small increase in intensity of the sharper peak in the spectrum from 10PC. Although no sharp component is seen in spectra from 5PC and 16PC after ARF6 binding, differences between the spectra after myr-ARF6 and non-ARF6 binding can still be discerned. For the spectra from 5PC, the ratio of positive peak intensity  $I_+$  to negative peak intensity  $I_-$  of the central peak,  $I_+/I_-$  (see Fig. 3), is 1.45 for the spectrum before ARF6 binding and 1.44 for the spectrum after non-ARF6 binding, essentially the same as the former, but it increases significantly to 1.58 for the spectrum after myr-ARF6 binding. For the spectra from 16PC, the ratio of the peak-peak intensity of the low-field line to the peak-peak intensity of central line  $I_{+1}/I_0$  (see Fig. 3) is the same for the spectra before and after non-ARF6 binding, 0.81, but it increases signifi-

cantly to 0.87 for the spectrum after myr-ARF6 binding. In sum, the spectra from 5PC and 16PC remain nearly the same after non-ARF6 binding but change significantly after myr-ARF6 binding.

To resolve the sharper component from the broad component, a simple method is spectral subtraction, i.e., subtracting the spectrum before myr-ARF6 binding from the corresponding spectrum after myr-ARF6 binding. The difference spectra of DPPTC and 10PC thus obtained are plotted in Fig. 4, A and B, respectively. For purposes of comparison, a spectrum from 4PT in DOPC dispersion in the presence of excess water is shown in Fig. 4 C. From Fig. 4, we can see the following. 1) The difference spectrum from 10PC (Fig. 4 B, solid line) has a normal line shape typical of a slow motional ESR spectrum, whereas the difference spectrum from DPPTC (Fig. 4 A) is severely distorted. This indicates that the main broad component in the spectrum from DPPTC after myr-ARF6 binding may be significantly different from the spectrum before myr-ARF6 binding. 2) Although the spectrum from 4PT (Fig. 4 C) is a fast-motion spectrum, the difference spectra from DPPTC and 10PC are not. It means that the latter signals are coming from DPPTC and 10PC exclusively dispersed in membranes. The information revealed from spectral subtractions is useful but is limited. To get quantitative information on dynamics and ordering of the lipid bilayers, NLLS fits to experimental spectra were conducted.

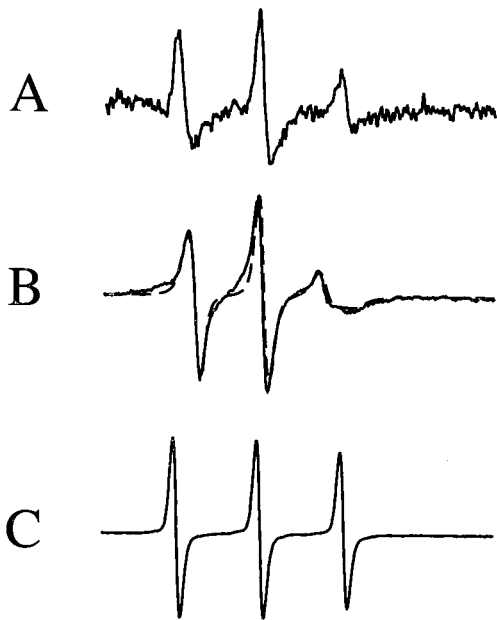


FIGURE 4 (A) The difference spectrum of DPPTC in the dispersion obtained by subtracting the spectrum before myr-ARF6 binding from the spectrum after myr-ARF6 binding; (B) The difference spectrum of 10PC in the dispersion obtained by subtracting the spectrum before myr-ARF6 binding from the spectrum after myr-ARF6 binding (—) and the sharp component of the simulation for the spectrum of 10PC after m-ARF6 binding obtained from NLLS fit (---); (C) The spectrum from 4PT in the DOPC dispersion in the presence of excess water.

### A summary of best-fit parameters from NLLS analyses

NLLS simulations were performed on spectra from DPPTC and 10PC before and after myr-ARF6 binding. The simulations (dashed lines) are superimposed on the corresponding experimental spectra (solid lines) in Fig. 3. All the spectra were simulated with two components except the one from DPPTC before myr-ARF6 binding, which was simulated with only one component. The two components obtained for each fit are plotted as inserts at the upper right corner of the corresponding experimental spectra in Fig. 3. The best fit parameters obtained from the simulations are listed in Table 1. Some features about the ordering and dynamics of the spin labels revealed from these results are summarized as follows. 1) The values of  $S$  of all sharp components in spectra from both DPPTC and 10PC, either before or after ARF6 binding, 0.15–0.23, are much lower than those of the corresponding broad components, 0.37–0.40 (10PC) or 0.65 (DPPTC). Thus, sharp components always have much lower ordering than broad components. We ascribe the sharp components to spectra generated from spin labels located in defects of bilayers, as will be discussed below. 2) The population of the sharp component in spectra from 10PC increases slightly from 0.11 before ARF6 binding to 0.13 after non-ARF6 binding and in-

TABLE 1 Best-fit parameters of  $R_{\perp}$  and  $S$  from NLLS fits for ESR spectra of DPPTC and 10PC in the dispersion before and after myr-ARF6 and non-ARF6 binding

Sample	Component	$R_{\perp}$ ( $s^{-1}$ )	$S$	Population
DPPTC				
Before binding		$6.26 \times 10^7$	0.40	
After myr-ARF6 binding	1	$5.87 \times 10^7$	0.65	0.87
	2	$2.00 \times 10^8$	0.23	0.13
10PC				
Before binding	1	$1.34 \times 10^8$	0.39	0.89
	2	$1.69 \times 10^8$	0.18	0.11
After non-ARF6 binding	1	$1.20 \times 10^8$	0.40	0.87
	2	$2.34 \times 10^8$	0.15	0.13
After myr-ARF6 binding	1	$1.24 \times 10^8$	0.37	0.82
	2	$2.18 \times 10^8$	0.16	0.18

The least-squares estimated error in  $R_{\perp}$  is  $\pm 5\%$  and in  $S$  is  $\pm 0.01$ .

creases significantly to 0.18 after myr-ARF6 binding. This indicates that myr-ARF6 has a stronger interaction with the membrane than non-ARF6 does. 3) The difference in  $R_{\perp}$  for spectra from 10PC before and after ARF6 binding is small. For broad components, the values of  $R_{\perp}$  are  $1.34 \times 10^8 s^{-1}$  before ARF6 binding vs.  $1.20 \times 10^8 s^{-1}$  after non-ARF6 binding and  $1.24 \times 10^8 s^{-1}$  after myr-ARF6 binding. They are in essence the same. For sharp components, it increases slightly from  $1.69 \times 10^8 s^{-1}$  before ARF6 binding to  $2.34 \times 10^8 s^{-1}$  after non-ARF6 binding and  $2.18 \times 10^8 s^{-1}$  after myr-ARF6 binding. For DPPTC, there is little change in  $R_{\perp}$  for the broad component ( $6.26 \times 10^7 s^{-1}$  before and  $5.87 \times 10^7 s^{-1}$  after ARF6 binding), whereas the sharp component that emerges after myr-ARF6 binding exhibits an increase to  $2.00 \times 10^8 s^{-1}$ . In summary, the effect of ARF6 binding on the membrane dynamics is relatively small, but the sharp component for DPPTC displays a significantly faster rate (by a factor of  $\sim 3$ ) than the broad component.

Just as we expected, the  $S$  value of the broad component in the spectrum from DPPTC after myr-ARF6 binding, 0.65, is much larger than that of the spectrum from DPPTC before myr-ARF6 binding, 0.40. That explains why the difference spectrum for DPPTC (Fig. 4 A) is distorted. The reason the difference spectrum for 10PC looks normal also becomes clear. 1) Both the motional and ordering parameters for the broad and narrow components before and after myr-ARF6 binding are nearly the same. 2) The major difference between the spectra before and after myr-ARF6 binding is an increase in relative population of the narrow component versus the broad components. We superimpose the sharp component for the spectrum from 10PC after myr-ARF6 binding obtained from NLLS fitting (dashed line) on the difference spectrum of 10PC (solid line) (cf. Fig. 4 B). It is seen that the two spectra are very similar. It turns out that results from the detailed NLLS fitting and from the simple spectral subtraction are consistent, in this case, as they should be.

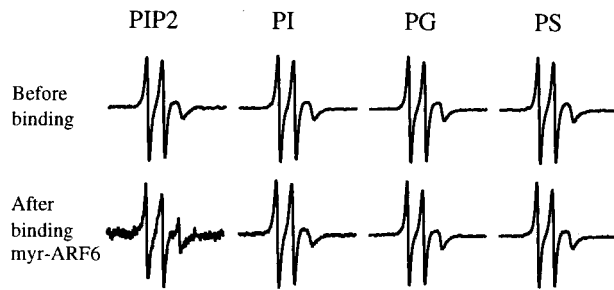


FIGURE 5 ESR spectra from DPPTC in dispersions containing different negatively charged lipids: PIP<sub>2</sub>, PI, DOPG, and DOPS before and after myr-ARF6 binding. The lipid to myr-ARF6 ratio is 1700.

### Myr-ARF6 binding to dispersions in which PIP<sub>2</sub> is replaced by PI, PG, or PS

ESR spectra from DPPTC in dispersions containing different negatively charged lipids, PIP<sub>2</sub>, PI, DOPG, and DOPS, before and after myr-ARF6 binding are compared in Fig. 5. The composition of the dispersions except for the one containing PIP<sub>2</sub> is POPE:DPPC:PI (or PG or PS):CHOL = 114:11:18:1.6. The amount of PI (or DOPG or DOPS) in the dispersions is tripled in comparison with the amount of PIP<sub>2</sub> that was used, to normalize the surface negative charge density in the dispersions containing PI (or DOPG or DOPS) to those containing PIP<sub>2</sub>. The lipid-to-protein molar ratio for all these bindings is 1700:1. As shown in Fig. 5, when PIP<sub>2</sub> is replaced by PI or DOPG or DOPS (with molar ratios normalized for charge), the spectra before and after myr-ARF6 binding are nearly identical. No sharp peak emerges in the spectra after myr-ARF6 binding.

### Bindings of r17-myr-ARF6, r17-non-ARF6, CDC42, and cytochrome C to the dispersion

Fig. 6 shows ESR spectra from DPPTC in dispersions before and after binding of r17-myr-ARF6, r17-non-ARF6, CDC42, and cytochrome C with lipid-to-protein ratios of 1000, 1000, 350, and 1400, respectively. In all cases, the spectra after binding are essentially identical to that before binding. This suggests that effects of myr-ARF6 binding on the structure of lipid bilayers are highly specific and not mimicked by proteins with similar charge (cytochrome C), posttranslational modification (r17-myr-ARF6 and r17-non-ARF6), or even other members of the RAS GTPase superfamily that binds to PIP<sub>2</sub> (Zheng et al., 1996). (In addition, these serve as control experiments that further rule out the likelihood of artifacts from spin labels not in the membrane phase when myr-ARF6 is used.)

### Binding of myr-ARF6 to LUVs of DOPC/PIP<sub>2</sub> (molar ratio of 95:5) and of pure DOPC

The dispersion samples we have used contain a high concentration of POPE, which is a non-lamellar phase forming

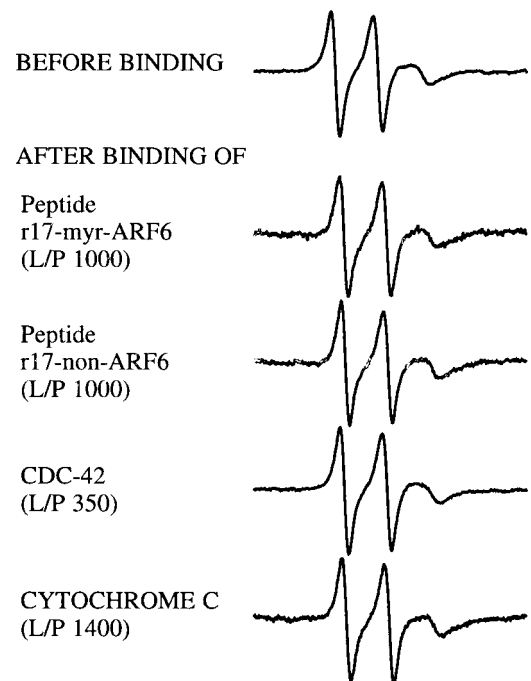


FIGURE 6 ESR spectra from DPPTC in dispersions before and after binding of r17-myr-ARF6, r17-non-ARF6, CDC42, and cytochrome C.

lipid. We have therefore also studied the binding of myr-ARF6 to vesicles composed of DOPC/PIP<sub>2</sub> (molar ratio of 95:5) and of pure DOPC at a lipid-to-myr-ARF6 molar ratio 500. Here we used LUV samples, because LUVs provide a better model membrane system compared with actual cells. The results are shown in Fig. 7, where a small sharper peak (indicated by an arrow) is seen only in the ESR spectrum from DPPTC in the LUV containing PIP<sub>2</sub>, not in the spectrum from the LUV of pure DOPC after the same amount of myr-ARF6 is added to both LUVs. The ESR spectra from

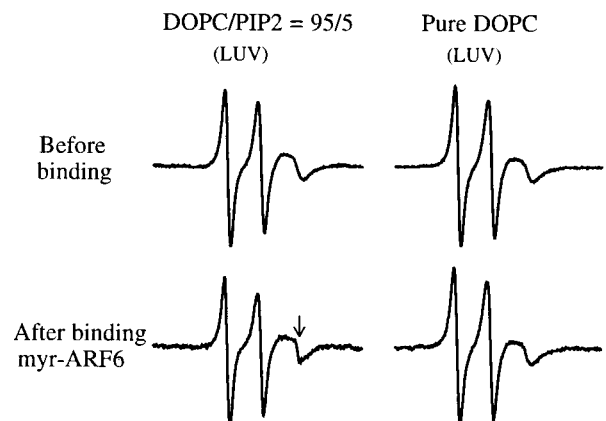


FIGURE 7 ESR spectra from DPPTC in LUVs of DOPC:PIP<sub>2</sub> = 95:5 and of pure DOPC before and after binding myr-ARF6. The molar ratio of lipid to myr-ARF6 L/P is 500. The arrow indicates that a sharp peak emerges after myr-ARF6 binding to the LUV of DOPC:PIP<sub>2</sub> = 95:5.

LUVs of pure DOPC before and after myr-ARF6 binding are nearly identical. Clearly, the interaction between myr-ARF6 and PIP<sub>2</sub> is responsible for the sharper peak. Thus, the presence of a high concentration of PE is not necessary for the emergence of the sharper peak, but PIP<sub>2</sub> is the key lipid ingredient to interact with myr-ARF6 to induce membrane defects. A matter of practical importance is the extent to which sharper peaks can be generated. We argue below that these sharper peaks are associated with defect formation in the bilayer, but if only a modest number are generated in a biochemical process, then it may be difficult to detect them. It would appear that the PE-containing vesicles enhance or amplify the sharper components to make the study more convenient.

This is not the first report of sharper components in ESR spectra from lipid bilayers. Occasionally, sharper components in ESR and <sup>31</sup>P NMR spectra appear in the literature, but the interpretation of these changes in spectra has been controversial. A major objective of this paper is to clarify the significance of these sharper components and to provide insights into the effects of ARF6 binding on membranes. Thus, it would be instructive to include ESR data we obtained from other spin-labeled membrane systems, which also show sharper components in the spectra as a result of lipid-lipid and lipid-protein interactions. Let us first consider the simplest membrane system, a pure DPPC dispersion.

### Sharper peaks in ESR and <sup>31</sup>P NMR spectra from lipid dispersions

ESR spectra of 10PC in DPPC dispersions in the presence of excess water at temperatures from -20°C to 45°C are plotted in Fig. 8. Sharper components emerge in the spectra only between 0°C and 20°C, which are superimposed on broadened main components. A sharper component in the spectrum from 8PC (also referred to as 7,6-PC in the literature (Spink et al., 1990)) in DPPC dispersions, which is very similar to that shown in Fig. 8, was observed at room temperature by Spink et al. (1990). They interpreted the two-component spectrum as evidence for coexistence of gel and liquid-crystalline phases in DPPC bilayers. If correct, the sharper peak in the spectra from 10PC in DPPC dispersion should persist and grow stronger when the temperature is raised, until the gel-to-liquid-crystalline phase transition temperature ( $T_c$ ), 41°C, is reached. However, the sharper peak fades away above 30°C, which does not support the two-phase coexistence explanation. We suggest that the sharp peaks in ESR spectra from 10PC and 8PC in DPPC dispersions reflect defects near the C10 position in the acyl-chain region of the DPPC bilayers. Alternatively, the 10PC spin labels are more effective at seeking out defect regions, e.g., they are less soluble in the membranes (Earle et al., 1994). Because defects are typically created by

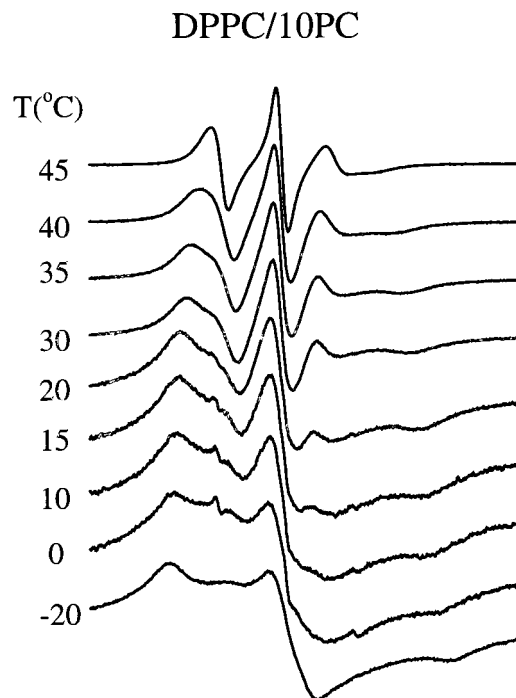


FIGURE 8 Temperature-dependent ESR spectra from 10PC in DPPC dispersion in the presence of excess water.

stresses in bilayers, their existence does not have to be consistent with a certain phase structure of the bilayer.

A sharp isotropic peak superimposed on a main broad peak in <sup>31</sup>P NMR spectra was observed from DPPC dispersions at 50°C (above  $T_c$ ), from DSPC dispersions at 40°C (below  $T_c$ ) (Cullis et al. 1976), and from SM at 40°C (near and below  $T_c$ ) and 60°C (above  $T_c$ ) (Cullis and Hope, 1980), whereas no sharp peak was observed in <sup>31</sup>P NMR spectra from DSPC (Cullis et al., 1976) and SM (Cullis and Hope, 1980) at 20°C (far below  $T_c$ ). Obviously, there is no correlation between the sharp peak and the phase structure of lipid bilayers from which the sharp peak was observed. It was suggested that small unilamellar vesicles could give rise to sharp peaks in <sup>31</sup>P NMR spectra, such as were observed in the <sup>31</sup>P NMR spectra from SM and DPPC dispersions (Cullis et al. 1976; Cullis and Hope, 1980). However, these dispersions were prepared in a standard way without sonication. It is not likely that small unilamellar vesicles can be produced by such preparations. Therefore, we suggest that these sharp peaks in the <sup>31</sup>P NMR spectra originate from defects in the headgroup region of bilayers.

### Leakage of DPPC vesicles and defects in the bilayers

It was reported that DPPC vesicles are permeable to a fluorescence probe carboxyfluorescein (molecular weight ~460) (Duzgunes et al., 1983), and our 4PT/VC test agrees

with the report. We found that immediately after addition of VC (molecular weight 162) to a DPPC dispersion containing 0.5 mol % 4PT, ESR signals vanished from both the pellet and supernatant. In contrast, upon addition of VC to a DOPC dispersion containing 0.5 mol % 4PT, the ESR signal disappeared from the supernatant but not from the pellet. Interestingly, the ESR spectrum from 4PT in the supernatant of DOPC dispersion before addition of VC differs significantly from that of 4PT in the pellet 1 h after addition of VC (data not shown). This reveals that the dynamic structure in the inter-bilayer polar region is distinct from that in the bulk water phase and that DPPC bilayers exhibit much more leakage than DOPC bilayers.

These results are curious given that there are at least two reasons we might expect that DPPC bilayers are less permeable than DOPC bilayers. 1) Bilayers are packed more tightly in the gel phase than in the liquid-crystalline phase. Usually, bilayers in the gel phase are less permeable than bilayers in the liquid-crystalline phase (Fettiplace and Haydon, 1980). At 23°C, DPPC is in the gel phase, whereas DOPC is in the liquid-crystalline phase. 2) Introduction of unsaturated bonds into the acyl chain will increase the membrane permeability (Bittman and Blau, 1972; Straume and Litman, 1987). There is a C9-C10 double bond in each acyl chain of a DOPC molecule.

The contradiction between what we would expect and what we actually observed might be resolved by the suggestion that a structural defect, possibly a cavity, may exist in DPPC bilayers. Given that the sharper peak is observed in the ESR spectra from 8PC and 10PC but not observed in the spectra from 5PC and 16PC in DPPC dispersions, it is quite possible that this cavity is located at or near the C8-C10 position in DPPC bilayers, or else these labels more effectively migrate to the defect regions (cf. above). We note that our findings are consistent with a similar paradigm previously proposed by Gordeliy et al. (1991) based upon their neutron scattering observations on DPPC bilayers. We failed to observe a sharper component in the spectra from DPPTC in DPPC dispersions between 0°C and 50°C, but the sharp component appears in <sup>31</sup>P NMR spectra from DPPC. The reason for the discrepancy is possibly as follows. The population of the sharper component in the spectra from 10PC is less than 5%. Because the main component in the 10PC spectra is broad, the small sharper component is easily resolved. But the main component in the DPPTC spectra is much narrower than that in the 10PC spectra; thus, it is likely that the sharper component in the DPPTC spectra cannot be resolved.

### Lipid-lipid and lipid-protein interactions can change amount of defects in bilayers

To explore how defects in bilayers could be affected by varying lipid composition and interacting with proteins, Gm1 and CHOL were incorporated sequentially into DPPC

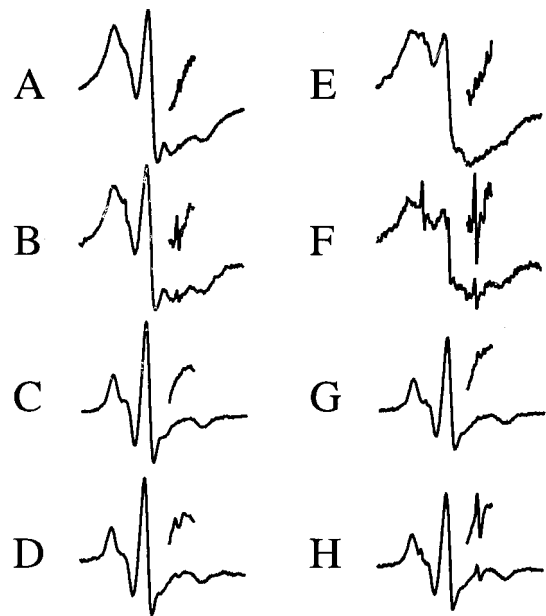


FIGURE 9 (A and E) ESR spectra from 10PC in pure DPPC and pure DSPC dispersions, respectively; (B and F) ESR spectra from 10PC in dispersions with composition DPPC:Gm1 = 9:1 and DSPC:Gm1 = 9:1, respectively; (C and G) ESR spectra from 10PC in dispersions with composition DPPC:Gm:CHOL = 9:1:10 and DSPC:Gm1:CHOL = 9:1:10, respectively; (D and H) ESR spectra from 10PC after CTB binding to the dispersions with composition DPPC:Gm:CHOL = 9:1:10 and DSPC:Gm1:CHOL = 9:1:10, respectively. The sharp peak at the high field wing of each spectrum is magnified by a factor of 3, so that the change in the intensity of these sharp peaks with the composition of the membrane can be seen clearly.

(DSPC) bilayers, and then CTB was added to the lipid mixture. An ESR spectrum was taken each time after the composition of the membranes was modified. All these spectra are plotted together and arranged in two columns in Fig. 9, A–H. The spectra from 10PC in pure DPPC (pure DSPC) dispersions is shown in Fig. 9 A (9 E), where the sharp components are clearly seen in both figures. Addition of 10 mol % Gm1 to DPPC (DSPC) dispersions increases the amplitude of the sharp component dramatically, as shown in Fig. 9 B (9 F). Upon addition of CHOL into the membrane consisting of DPPC(DSPC)/Gm1 = 9(9)/1, to bring it to 50 mol % CHOL, the sharp component almost disappears, as shown in Fig. 9 C (9 G). However, after binding of CTB to the membrane (DPPC(DSPC)/Gm1/CHOL = 9(9)/1/10), the sharp component emerges again as shown in Fig. 9 D (9 H). The implications of these results are the following. 1) The intensity of sharp components could be enhanced or depressed simply by varying the composition of the lipid bilayer; i.e., the amount of defect in the membrane could be altered by lipid-lipid interactions. CHOL is especially effective in eliminating defects in the acyl-chain region of bilayers. This is consistent with the well known ordering effect of CHOL on the bilayers (Bloom et al., 1991). That is, CHOL makes the packing of

acyl chain tight and reduces the permeability of bilayers (Bittman and Blau, 1972; Straume and Litman, 1987; Yan and Eisenthal, 2000). Interestingly, the sharp component in the <sup>31</sup>P NMR spectrum from pure SM at 60°C disappears after incorporating equimolar CHOL into SM (Cullis and Hope, 1980). It reveals that CHOL can also reduce defects in the headgroup region of bilayers. 2) Lipid-protein interactions can also significantly induce defect formation in membranes. This has been typified by observations of fusion pores in plasma membranes generated by insertion of fusion peptide into the membrane in the virus-cell fusion process. Although there has not yet been any report of an ESR observation of fusion pores, the sharp component in the ESR spectrum from a spin-labeled stearic acid incorporated in DTPG bilayers emerged after addition of melittin (Kleinschmidt et al., 1997), so this may serve as a good example for membrane defects induced by lipid-protein interactions. Because it is known that melittin, a positively charged peptide, is lytic, fusogenic (Dufourcq et al., 1986), and capable of inducing a non-lamellar phase (Batenburg et al., 1987), it is very likely that the sharp component in the ESR spectrum from spin-labeled stearic acid after melittin binding to DTPG bilayers arises from defects created in the DTPG bilayers.

## DISCUSSION

### Specific interactions between PIP<sub>2</sub> and myr-ARF6 and defects in membranes

As shown in Fig. 5 (lower row), among the four spectra of DPPTC in dispersions containing different negatively charged lipids after myr-ARF6 binding, the sharp component is seen only in the one containing PIP<sub>2</sub>, not in the others in which PIP<sub>2</sub> is replaced by PI or PG or PS. This clearly indicates that only in the membrane containing PIP<sub>2</sub> can defects be induced in the headgroup region upon GDP-bound myr-ARF6 binding. In other words, specific interactions between GDP-bound myr-ARF6 and PIP<sub>2</sub> do exist that are responsible for the defect formation in bilayers. Shiffer et al. (1998) found that PIP<sub>2</sub> in RBC membrane can redistribute intracellular cations and lead to loss of phospholipid asymmetry. Their findings suggest that PIP<sub>2</sub> induces pore formation in RBC membrane. Given that the chemical compositions of the RBC membrane differ greatly from the model membranes we used in this work, which have simple lipid compositions, it seems that the formation of defects in all these structures is a function of the presence of PIP<sub>2</sub>. It is tempting to speculate that the mechanism for defect formation in the model membrane and the mechanism for pore formation in RBC membrane might be similar. Moreover, the specificity in the GDP-bound myr-ARF6/PIP<sub>2</sub> interaction is further demonstrated by the inability to generate such defects in the dispersion containing PIP<sub>2</sub> upon

addition of CDC42, which also binds to PIP<sub>2</sub> and is an activator of PLD (Singer et al., 1995).

### Mechanisms of ARF6 binding

It has been suggested that two mechanisms are responsible for myr-ARF binding to biological membranes: 1) the electrostatic interaction between a patch of positively charged amino residues in ARF and negatively charged headgroups of acidic lipids in the membrane and 2) the hydrophobic interaction through insertion of the attached acyl chain on the amino terminal of ARF into the bilayers. Both interactions acting together bind the protein tightly to the membrane surface (reviewed by McLaughlin and Aderem, 1995). As shown in Fig. 3, ESR spectra from all four spin labels (DPPTC, 5PC, 10PC, and 16PC) show little or small changes upon non-ARF6 binding but large changes upon myr-ARF6 binding. This is consistent with the observation that myr-ARF5 binds to Golgi membranes, whereas non-ARF does not (Haun et al., 1993). In addition, Fig. 6 shows that ESR spectra from DPPTC remain unchanged upon binding of cytochrome C, a positively charged protein, and upon binding of r17-myr-ARF6, a myristoylated peptide, to the dispersion. Taken together, these results suggest that electrostatic and hydrophobic interactions acting together can lead to significant alterations in membrane structure mediated via ARF proteins.

It was found that defects and density fluctuations in bilayers play a prominent role in modulating phospholipase A<sub>2</sub> activity (Burack et al., 1997). It was proposed that membrane fusion can be induced by defects in lipid bilayers (Hui et al., 1981). Our present results suggest that defects in bilayers are generated by specific interactions between ARF6 and PIP<sub>2</sub>, which are both involved in the activation of PLD (reviewed in Singer et al., 1996; Exton, 1999; Frohman et al., 1999). The significance of generation of membrane defects on vesicles by ARF may include 1) providing a direct access to the substrate in the membrane for phospholipases; 2) increasing the permeability of the membrane to allow trans-bilayer movement of key components of the enzyme catalytic process, i.e., dissipation of products and replenishment of substrates; 3) providing an initial fusion pore; 4) facilitating the budding vesicle to pinch off; 5) mediating other lipid-lipid and lipid-protein interactions essential to membrane remodeling. If defects are important for some membrane proteins to function, then a modification in lipid composition, which enhances or suppresses defects in lipid bilayers, may provide an essential mechanism for regulating these processes (Sen et al., 1991). Interestingly, the effects of ARF6 in our *in vitro* system did not require activation by GTP. The activation of monomeric G proteins by GTP is a molecular switch in signal transduction processes. It is possible that the role of ARF in creating bilayer defects in intact cells will require activation to initiate changes in subcellular localization, but such changes are not

necessary in this *in vitro* system. Considering the ubiquitous distribution of ARF proteins and the diversity of biological functions (e.g., cell signal transduction, endocytosis, exocytosis, and viral entry) with which it has been implicated, the creation of membrane defects may be of central importance to these functions.

This study focuses on an important aspect of our main research goal: the effect of lipid-lipid and lipid-protein interactions on the dynamic structure of membranes. That is, we are exploring whether the plasma membrane plays an active role in various cellular processes. However, the composition and structure of plasma membranes are very complicated, for reasons that include the following. 1) Lipid-lipid, lipid-protein, and protein-protein interactions are often coupled with one another on the surface of or within plasma membrane. 2) Both the composition and the structure of plasma membrane are heterogeneous and dynamic; e.g., dynamic domain structures in plasma membrane were found to be involved in cell signal transduction (Field et al., 1995). Furthermore, it is likely that the amount of defect induced in a plasma membrane by lipid-lipid and lipid-protein interactions is small. This raises a question of sensitivity for detection. Thus, one can profit from a model system, in which the amount of defects is enhanced. This appears to be the case for the model membrane system used in our ESR study. It enables us to clearly demonstrate that only the interaction between PIP<sub>2</sub> and myr-ARF6 is responsible for the defect formation in the membrane. The high concentration of POPE probably enhances the effect of PIP<sub>2</sub>/myr-ARF6 interaction on the defect formation, but in the absence of PIP<sub>2</sub> (replaced by PG, PS, or PI), it does not lead to observable defect formation. In addition, substantial defects are induced in the LUVs of DOPC that contains PIP<sub>2</sub> upon myr-ARF6 binding. Therefore, PE is not essential for the defect formation seen by ESR.

We are extending this current study to biological membranes. It is encouraging to note that defects have been observed in large plasma membrane vesicles derived from rat basophilic leukemia (RBL) cells upon binding of myr-ARF6 (M. Ge, A. Costa-Filho, A. Gidwani, D. Holowka, B. Baird, H.A. Brown, and J.H. Freed, to be published). Thus, one may expect that myr-ARF6 binding could have a similar effect on the plasma membrane of the intact cells.

## CONCLUSIONS

Past research has suggested an interaction between myristoylated ARF6 and PIP<sub>2</sub>. This has been demonstrated in the present study by the formation of sharp components in the ESR spectrum from the headgroup-labeled DPPC after binding of myristoylated ARF6 to the vesicle dispersion but not from dispersions in which PIP<sub>2</sub> is replaced by PI, PS, or PG. This characteristic spectral component is not found in ESR spectra from DPPTC after addition of CDC42, synthesized peptides of residues 1–17 of myristoylated and non-

myristoylated human ARF6, or cytochrome C. We postulate that sharp components observed in ESR spectra from spin-labeled membranes arise from defects in the lipid bilayers, which are produced as a result of lipid-lipid and lipid-protein interactions. These findings suggest that ARF may play a major role in restructuring membranes and in preparation for events that require remodeling of biological membranes.

We thank Antonio Costa-Filho for his help in the ESR experiments.

This work received support from the Sidney Kimmel Foundation for Cancer Research, the USDA Hatch Act Consolidated Research Program, and the National Institutes of Health (grant GM58516 to H.A.B. and grant GM25862 to J.H.F.).

## REFERENCES

- Antonny, B., S. Beraud-Dufour, P. Chardin, and M. Chabre. 1997. N-terminal hydrophobic residues of G-protein ADP-ribosylation factor-1 insert into membrane phospholipids upon GDP to GTP exchange. *Biochemistry*. 36:4675–4684.
- Batenburg, A. M., J. C. L. Hibbeln, A. J. Verkleij, and B. de Kruijff. 1987. Melittin induced H<sub>II</sub> phase formation in cardiolipin model membranes. *Biochim. Biophys. Acta*. 903:142–154.
- Bittman, R., and L. Blau. 1972. The phospholipid-cholesterol interaction: kinetics of water permeability in liposomes. *Biochemistry*. 11: 4831–4839.
- Bloom, M., E. Evans, and O. G. Mouritsen. 1991. Physical properties of the fluid lipid-bilayer component of cell membranes: a perspective. *Q. Rev. Biophys.* 24:293–397.
- Brown, H. A., S. Gutowski, C. R. Moomaw, C. Slaughter, and P. C. Sternweis. 1993. ADP-ribosylation factor, a small GTP-dependent regulatory protein, stimulates phospholipase D activity. *Cell*. 75: 1137–1144.
- Brown, H. A., and P. C. Sternweis. 1995. Stimulation of phospholipase D by ADP-ribosylation factor. *Methods Enzymol.* 257:313–324.
- Budil, D. E., S. Lee, S. Saxena, and J. H. Freed. 1996. Nonlinear-least-squares analysis of slow-motion EPR spectra in one and two dimensions using a modified Levenberg-Marquardt algorithm. *J. Magn. Reson.* A120:155–189.
- Burack, W. R., A. R. G. Dibble, M. M. Allietta, and R. L. Biltonen. 1997. Changes in vesicle morphology induced by lateral phase separation modulate phospholipase A<sub>2</sub> activity. *Biochemistry*. 36:10551–10557.
- Carrington, A., and A. D. McLachlan. 1967. Introduction to Magnetic Resonance with Applications to Chemistry and Chemical Physics. Harper and Row, New York.
- Chen, Y. G., A. Siddhanta, C. D. Austin, S. M. Hammond, T. C. Sung, M. A. Frohman, A. J. Morris, and D. Shields. 1997. Phospholipase D stimulates release of nascent secretory vesicles from the trans-Golgi network. *J. Cell Biol.* 138:495–504.
- Cohen, J. S., and H. A. Brown. 2001. Phospholipases stimulate secretion in RBL mast cells. *Biochemistry*. 40:6589–6597.
- Cockcroft, S., G. M. H. Thomas, A. Fensome, B. Geny, E. Cunningham, I. Gout, I. Hiles, N. F. Totty, O. Truong, and J. J. Hsuan. 1994. Phospholipase D: a downstream effector of ARF in granulocytes. *Science*. 263:523–526.
- Cullis, P. R., B. De Kruijff, and R. E. Richards. 1976. Factors affecting the motion of the polar headgroup in phospholipid bilayers: a <sup>31</sup>P NMR study of unsonicated phosphatidylcholine liposomes. *Biochim. Biophys. Acta*. 426:433–446.
- Cullis, P. R., and M. J. Hope. 1980. The bilayer stabilizing role of sphingomyelin in the presence of cholesterol: a <sup>31</sup>P NMR study. *Biochim. Biophys. Acta*. 597:533–542.

- Dufourcq, J., J.-F. Faucon, G. Fourche, J.-L. Dasseux, M. L. Maire, and T. Gulik-Krzywicki. 1986. Morphological changes of phosphatidylcholine bilayers induced by melittin: vesicularization, fusion, discoidal particles. *Biochim. Biophys. Acta.* 859:33–48.
- Duzgunes, N., J. Wilschut, K. Hong, R. Fraley, C. Perry, D. S. Friend, T. L. James, and D. Papahadjopoulos. 1983. Physicochemical characterization of large unilamellar phospholipid vesicles prepared by reverse phase evaporation. *Biochim. Biophys. Acta.* 732:289–299.
- Earle, K. A., J. K. Moscicki, M. Ge, D. E. Budil, and J. H. Freed. 1994. 250-GHz electron spin resonance studies of polarity gradient along the aliphatic chains in phospholipid membranes. *Biophys. J.* 66:1213–1221.
- Exton, J. H. 1999. Regulation of phospholipase D. *Biochim. Biophys. Acta.* 1439:121–133.
- Field, K. A., D. Holowka, and B. Baird. 205. 1995. FceRI-mediated recruitment of p53/56<sup>lyn</sup> to detergent-resistant membrane domains accompanies cellular signaling. *Proc. Natl. Acad. Sci. U.S.A.* 92: 9201–9209.
- Fettiplace, R., and D. A. Haydon. 1980. Water permeability of lipid membranes. *Physiol. Rev.* 60:510–550.
- Franco, M., P. Chardin, M. Chabre, and S. Paris. 1995. Myristoylation of ADP-ribosylation factor 1 facilitates nucleotide exchange at physiological Mg levels. *J. Biol. Chem.* 270:1337–1341.
- Freed, J. H. 2000. New technologies in electron spin resonance. *Annu. Rev. Phys. Chem.* 51:655–689.
- Freyberg, Z., D. Sweeney, A. Siddhanta, S. Bourgoïn, M. Frohman, and D. Shields. 2001. Intracellular localization of phospholipase D1 in mammalian cells. *Mol. Biol. Cell.* 12:943–955.
- Frohman, M. A., T.-C. Sung, and A. J. Morris. 1999. Mammalian phospholipase D structure and regulation. *Biochim. Biophys. Acta.* 1439: 175–186.
- Ge, M., and J. H. Freed. 1999. Electron-spin resonance study of aggregation of gramicidin in dipalmitoylphosphatidylcholine bilayers and hydrophobic mismatch. *Biophys. J.* 76:264–280.
- Ge, M., D. E. Budil, and J. H. Freed. 1994. An electron spin resonance study of interaction between phosphatidylcholine and phosphatidylserine in oriented membrane. *Biophys. J.* 66:1515–1521.
- Gordeliy, V. I., V. G. Ivkov, Y. M. Ostanevich, and L. S. Yaguzhinskiij. 1991. Detection of structural defects in phosphatidylcholine membranes by small-angle neutron scattering: the cluster model of a lipid bilayer. *Biochim. Biophys. Acta.* 1061:39–48.
- Haun, R. S., S. C. Tsai, R. Adamik, J. Moss, and M. Vaughan. 1993. Effect of myristoylation on GTP-dependent binding of ADP-ribosylation factor to Golgi. *J. Biol. Chem.* 268:7064–7068.
- Hong, J. X., R. S. Haun, S. C. Tsai, J. Moss, and M. Vaughan. 1994. Effect of ADP-ribosylation factor amino-terminal deletion on its GTP-dependent stimulation of cholera toxin activity. *J. Biol. Chem.* 269: 9743–9745.
- Hui, S. W., T. P. Stewart, and L. T. Boni. 1981. Membrane fusion through point defects in bilayers. *Science.* 212:921–923.
- Israelachvili, J. 1991. *Intermolecular and Surface Forces*, 2nd ed. Academic Press, London.
- Ivanova, P. T., B. A. Cerda, D. M. Horn, J. S. Cohen, F. W. McLafferty, and H. A. Brown. 2001. Electrospray ionization mass spectrometry analysis of changes in phospholipids in RBL-2H3 mastocytoma cells during degranulation. *Proc. Natl. Acad. Sci. U.S.A.* 98:7152–7157.
- Jones, D., C. Morgan, and S. Cockcroft. 1999. Phospholipase D and membrane traffic: potential roles in regulated exocytosis, membrane delivery and vesicle budding. *Biochim. Biophys. Acta.* 1439:229–244.
- Kleinschmidt, J. H., J. M. Mahaney, D. D. Thomas, and D. Marsh. 1997. Interactions of bee venom melittin with zwitterionic and negatively charged phospholipid bilayers: a spin-label electron spin resonance study. *Biophys. J.* 72:767–778.
- Ktistakis, N. T., H. A. Brown, M. G. Waters, P. C. Sternweis, and M. G. Roth. 1996. Evidence that phospholipase D mediates ADP ribosylation factor-dependent formation of Golgi coated vesicles. *J. Cell Biol.* 134: 295–306.
- Lodge, J. K., E. Jackson-Machelski, B. Devadas, M. E. Zupiec, D. P. Getman, N. Kishore, S. K. Freeman, C. A. McWherter, J. A. Sikorski, and J. I. Gordon. 1997. N-myristoylation of ARF protein in *Candida albicans*: an in vivo assay for evaluating antifungal inhibitors of myristoyl-CoA: protein N-myristoyltransferase. *Microbiology.* 143: 357–366.
- McLaughlin, S., and A. Aderem. 1995. The myristoyl-electrostatic switch: a modulator of reversible protein-membrane interactions. *Trends Biochem. Sci.* 20:272–276.
- Meirovitch, E., D. Igner, G. Moro, and J. H. Freed. 1982. Electron-spin relaxation and ordering in smectic and supercooled nematic liquid crystals. *J. Chem. Phys.* 77:3915–3938.
- Meirovitch, E., A. Nayeem, and Jack H. Freed. 1984. Analysis of protein-lipid interactions based on model simulations of electron spin resonance spectra. *J. Phys. Chem.* 88:3454–3465.
- Patyal, B. R., R. H. Crepeau, and J. H. Freed. 1997. Lipid-gramicidin interactions using two-dimensional Fourier-transform electron spin resonance. *Biophys. J.* 73:2201–2220.
- Randazzo, P. A., O. Weiss, and R. A. Kahn. 1995. Preparation of recombinant ADP-ribosylation factor. *Methods Enzymol.* 257:128–135.
- Roth, M. G., and P. C. Sternweis. 1997. The role of lipid signaling in constitutive membrane traffic. *Curr. Opin. Cell Biol.* 9:519–526.
- Rothman, J. E. 1994. Mechanisms of intracellular protein transport. *Nature.* 372:55–63.
- Schneider, D. J., and J. H. Freed. 1989. Calculating slow motional magnetic resonance spectra: a user's guide. In *Spin Labeling Theory and Applications*, Vol. 8. L. J. Berliner and J. Reuben, editors. Plenum Press, New York. 1–76.
- Sen, A., T. V. Isac, and S.-W. Hui. 1991. Bilayer packing stress and defects in mixed dilinoleoylphosphatidylethanolamine and palmitoyl-oleoylphosphatidylcholine and their susceptibility to phospholipase A<sub>2</sub>. *Biochemistry.* 30:4516–4521.
- Shiffer, K. A., L. Rood, R. K. Emerson, and F. A. Kuypers. 1998. Effects of phosphatidylinositol diphosphate on phospholipid asymmetry in the human erythrocyte membrane. *Biochemistry.* 37:3449–3458.
- Shin, Y.-K., and J. H. Freed. 1989. Thermodynamics of phosphatidylcholine-cholesterol mixed model membranes in the liquid crystalline state studied by the orientational order parameter. *Biophys. J.* 56:1093–1100.
- Singer, W. D., H. A. Brown, G. M. Bokoch, and P. C. Sternweis. 1995. Resolved phospholipase D activity is modulated by cytosolic factors other than ARF. *J. Biol. Chem.* 270:14944–14950.
- Singer, W. D., H. A. Brown, X. Jiang, and P. C. Sternweis. 1996. Regulation of phospholipase D by protein kinase C is synergistic with ADP-ribosylation factor and independent of protein kinase activity. *J. Biol. Chem.* 271:4504–4510.
- Spink, C. H., M. D. Yeager, and G. W. Feigenson. 1990. Partitioning behavior of indocarbocyanine probes between coexisting gel and fluid phases in model membranes. *Biochim. Biophys. Acta.* 1023:25–33.
- Straume, M., and B. J. Litman. 1987. Equilibrium and dynamics of large, unilamellar, unsaturated acyl chain phosphatidylcholine vesicles: high order analysis of 1,6-diphenyl-1,3,5-hexatriene and 1-[4-(trimethylammonio)phenyl]-1,3,5-hexatriene anisotropy decay. *Biochemistry.* 26: 5113–5120.
- Sudhof, T. C. 1995. The synaptic vesicle cycle: a cascade of protein-protein interactions. *Nature.* 375:645–653.
- Terui, T., R. A. Kahn, and P. A. Randazzo. 1994. Effects of acid phospholipids on nucleotide exchange properties of ADP-ribosylation factor 1: evidence for specific interaction with phosphatidylinositol 4,5-bisphosphate. *J. Biol. Chem.* 269:28130–28135.
- Walker, S. J., W.-J. Wu, R. A. Cerione, and H. A. Brown. 2000. Activation of phospholipase D1 by cdc42 requires the Rho insert region. *J. Biol. Chem.* 2000:15665–15668.
- Yan, E. C. Y., and K. B. Eisenhal. 2000. Effect of cholesterol on molecular transport of organic cations across liposome bilayers probed by second harmonic generation. *Biophys. J.* 79:898–903.
- Zheng, Y., J. A. Glaven, W. J. Wu, and R. A. Cerione. 1996. Phosphatidylinositol 4,5-bisphosphate provides an alternative to guanine nucleotide exchange factors by stimulating the dissociation of GDP from Cdc42Hs. *J. Biol. Chem.* 271:23815–23819.